RESEARCH ARTICLE

Multivariate indium–organic frameworks for highly efficient carbon dioxide capture and electrocatalytic conversion†

Shuo Wang, Ying Wang, [ID] Jia-Min Huo, Wen-Yu Yuan, [ID] * Peng Zhang, Shu-Ni Li [ID] and Quan-Guo Zhai [ID] *

It is crucial to design highly selective and cost-effective materials for efficient CO_2 uptake and the desirable transformation of CO_2 into fuels or high-value chemical products. Here, we synthesize a series of trinuclear indium cluster-based metal–organic frameworks (MOFs) for highly efficient CO_2 capture and electrocatalytic conversion into C_1 products. By adjusting the metal type and replacing the ligand, the mixed metal-based MOF InCo-ABDBC-HIN shows high CO_2 capture performance (101.7 cm^3 g^{-1} at 273 K under low pressure) and superior activity (a maximum FE_{C_1} of 81.5% at −2.2 V *vs.* Ag/Ag$^+$) for electrocatalytic CO_2 reduction in organic electrolytes due to its modified electronic structure. Theoretical calculations suggest that the substitution of In by Co significantly modified the electronic structure of In-based clusters, which provides rich unpaired electrons for the CO_2RR and enhances the charge transfer efficiency. This work provides a specially coordinated trinuclear indium cluster-based MOF and sheds new light on the precise structural design of both CO_2 adsorbents and electrocatalysts for efficient CO_2 reduction.

Introduction

Reducing the atmospheric CO_2 concentration is one of the most important scientific research goals at present.[1] Besides reducing CO_2 emissions *via* replacing fossil fuels using low-carbon or non-carbon clean energy, CO_2 capture and conversion is considered as a promising strategy to reduce the CO_2 concentration. Compared with the direct reduction of CO_2 emissions *via* CO_2 capture and storage, converting CO_2 into fuels,[2,3] such as carbon monoxide,[4,5] methane,[6–8] formate,[9,10] ethylene[11–13] and ethanol[14–17] is considered as a promising strategy to mitigate the greenhouse effect. Nevertheless, the conversion of CO_2 into high value-added products suffers from the slow kinetic reaction, the competitive hydrogen evolution reaction (HER), and poor Faraday efficiency (FE) and product selectivity.[18] Thus, the exploration of highly efficient and highly selective catalysts for the CO_2 reduction reaction (CO_2RR) is extremely urgent.[19–22]

Metal–organic frameworks (MOFs), as porous crystalline materials composed of multifarious organic linkers and metal-rich nodes,[23–26] provide abundant active sites for CO_2 adsorption and electrocatalytic reaction. The tailorable nature and their structural diversity make them ideal candidates for CO_2 capture and conversion. Compared to other adsorbents, the ultra-high surface area of MOFs provides an excellent ability to absorb CO_2 by physical adsorption methods. The tailorable chemical environments, such as the coordination number and oxidation values, provide insight into the precise design of a structure for a highly efficient electrocatalytic CO_2RR and high selectivity for the final products.[27,28] However, there are a number of important limitations that need to be addressed when applying MOFs to electrochemical applications, primarily their poor stability and conductivity.[29]

Among various MOF-based catalysts, indium (In)-based catalysts with low toxicity and environmental friendliness show high selectivity towards formate production.[30–34] Substantial works demonstrated that the electrochemical performance can be improved *via* the modification of the chemical environment of In-based MOFs *via* the precise control of the metal species and organic ligands. For example, Ding *et al.* reported an original In-MOF by the incorporation of redox-active organic linkers, which enhanced the electrocatalytic activity for the CO_2RR to $HCOO^-$ with a highly improved FE_{HCOO^-} (from 54.7% to 89.6%).[35] Xia *et al.* reported a peer-to-peer strategy for modular assembly of In-based catalysts by amino functionalization, which demonstrated a high FE of 94.4% for CO_2 electroreduction.[36] In addition, incorporating a second

Key Laboratory of Macromolecular Science of Shaanxi Province, Key Laboratory of Applied Surface and Colloid Chemistry, Ministry of Education, School of Chemistry & Chemical Engineering, Shaanxi Normal University, Xi'an, Shaanxi, 710062, China. E-mail: wenyu.yuan@snnu.edu.cn, zhaiqg@snnu.edu.cn
†Electronic supplementary information (ESI) available. See DOI: https://doi.org/10.1039/d2qi02020c

158 | *Inorg. Chem. Front.*, 2023, **10**, 158–167

This journal is © the Partner Organisations 2023

metal to form bimetallic compounds has been proved to be an efficient strategy to promote the electrocatalytic activity of various catalysts (*e.g.* metal oxides, metal nitrides, and single-atom catalysts). For example, Rasul *et al.* constructed a Cu–In alloy by electrodepositing a thin layer of In on oxide-derived copper, which exhibited a high selectivity of 95% towards CO.[37] Thus, the bimetallic regulation of In-based MOFs is promising to regulate the electrocatalytic CO_2 reduction performance. As a matter of fact, heterometallic In-MOFs have been reported for a wide range of applications, including N_2 reduction,[38] catalytic hydrogenation reduction of CO_2,[39] multiple ion detection[40] and photocatalytic fixation.[41] However, to the best of our knowledge, bimetallic engineering on In-based MOFs as catalysts for the CO_2RR has not been reported to date.

Here, we report a unique trinuclear cluster In-based MOF (InCo-ABDBC-HIN), in which each trinuclear cluster is eight-coordinated, as an efficient CO_2RR catalyst and precise structural control was carried out to optimize the activity. Compared with the widely reported nine-coordinated structure, the unusual eight-coordinated environment provides a non-coordinate site for the adsorption of intermediates, which is promising to demonstrate enhanced electrocatalytic activity. The metal (In-ABDBC-HIN) and the functional groups in ligands (In-ABDBC-HAIN) are further regulated to boost the CO_2RR performance. The results demonstrate that the introduction of Co to a partially substituted indium atom (InCo-ABDBC-HIN) enables efficient production of C_1 products from the CO_2RR on account of the modified electronic structure of the active sites. The current density under an applied potential of −2.2 V *vs.* Ag/Ag^+ reached up to 21.2 mA cm^{-2}, while a high FE of 81.5% for C1 products is achieved. Density functional theory (DFT) calculations uncover that the $InCo_2$-based structure exhibits improved unpaired electronic distribution and enhanced electrical conductivity, while the amino group suppresses the electrical conductivity, thereby resulting in the high CO_2RR activity of InCo-ABDBC-HIN. The reported novel trinuclear indium cluster-based MOF is also promising as an efficient catalyst for photocatalysis, thermo-catalysis, and other electrocatalytic reactions.

Experimental

Chemicals

The following chemicals were used as received without further purification: indium nitrate hydrate (In(NO$_3$)$_3$·xH$_2$O, >99%), cobalt nitrate hexahydrate (Co(NO$_3$)$_2$·6H$_2$O, >99%), isonicotinic acid (HIN, >99%) and 2-aminoisonicotinic acid (HAIN, >97%) were purchased from Aladdin Bio-Chem Technology Co., Ltd (Shanghai, China). *N,N*-Dimethylformamide (DMF), sulfuric acid (H$_2$SO$_4$, 95%–98%) and acetonitrile (CH$_3$CN) were purchased from Sinopharm Chemical Reagent Co. Ltd (Shanghai, China). The Nafion D-520 dispersion (5 wt% in lower aliphatic alcohols and water), the Nafion 117 proton exchange membrane and a gas diffusion layer (GDL) were purchased from Shanghai Hesen Electric Co.

Synthesis

Synthesis of 4,4′-azobenzenedicarboxylic acid (H$_2$ABDBC). H$_2$ABDBC was synthesized in accordance with the previously reported method.[42] 4-Nitrobenzoic acid (7.5 g) and sodium hydroxide (25 g) were dissolved in 200 ml deionized water, then added to a 500 ml flask and heated at 50 °C. 3.7 M glucose is stirred and dissolved in an aqueous solution (75 mL), and then added to a round-bottomed flask. The reaction was stirred for 10 minutes, and then cooled to room temperature (RT). After stirring the solution in air for 12 hours, a proper amount of acetic acid solution was added to precipitate H$_2$ABDBC (Fig. S4†).

Synthesis of In-ABDBC-HIN. In-ABDBC-HIN was synthesized following the previously reported method.[43] In(NO$_3$)$_3$·xH$_2$O (0.060 g), H$_2$ABDBC (0.027 g), and HIN (0.012 g) were sequentially added to a 20 mL vial, followed by 5 mL DMF, which was stirred until complete dissolution. The vial was heated at 80 °C for 3 days. The orange polyhedral crystals were washed three times with fresh DMF and acetonitrile.

Synthesis of InCo-ABDBC-HIN. In (NO$_3$)$_3$·xH$_2$O, Co (NO$_3$)$_2$·6H$_2$O (0.029 g), H$_2$ABDBC (27.0 mg), and HIN (0.012 mg) were mixed with the solvent of 5 mL of DMF. The vial was heated in an 80 °C oven for 3 days. The red polyhedral crystals were washed with fresh DMF and acetonitrile three times. The molecular formula is (In$_3$O)(OH)(ABDBC)$_2$(HIN)$_2$ H$_2$O.

Synthesis of In-ABDBC-HAIN. A mixture of In(NO$_3$)$_3$·xH$_2$O (0.060 g), H$_2$ABDBC (0.027 g), and HAIN (0.014 g) was heated at 80 °C for 3 days. Sequentially, the orange polyhedral crystals were collected and washed with DMF and acetonitrile three times.

Sample activation

The as-synthesized samples of InCo-ABDBC-HIN were immersed in acetonitrile for 3 days and acetonitrile was refreshed every 12 hours. Then, the InCo-ABDBC-HIN samples exchanged with acetonitrile were activated under vacuum at 373 K for 8 h. The sample activation conditions of In-ABDBC-HIN and In-ABDBC-HAIN were the same as those of InCo-ABDBC-HIN.

Characterization

X-ray diffraction (XRD) was performed on a MiniFlex 600 (Rigaku Co. Ltd, Japan) with Cu Kα radiation from 4 to 80° ($λ$ = 1.5406 Å). Field emission scanning electron microcopy (FE-SEM) images were obtained on an SU8220 spectrometer (Hitachi Co. Ltd, Japan) under a voltage of 10 kV. Thermogravimetric analysis (TGA) experiments were conducted on a HCT-1 (Hengjiu Co. Ltd, Beijing). Thermo analyzer tested in the atmosphere of N_2 (RT–800 °C). Fourier transform infrared (FT-IR) measurements were performed on a TENSOR II spectrometer (Bruker Co. Ltd, Germany) with KBr pellets. The metallic elements in the samples and the electrolyte were obtained *via* ICP-MS using an Agilent 7800 (Agilent Co. Ltd, US)

This journal is © the Partner Organisations 2023

Inorg. Chem. Front., 2023, **10**, 158–167 | **159**

Electrochemical measurements

The electrodes In-ABDBC-HIN, InCo-ABDBC-HIN and In-ABDBC-HAIN were prepared using the same protocol. 20 mg of MOF was suspended in 900 μL isopropanol with 100 μL Nafion D521 dispersion (5 wt%) assisted by ultrasound sonication for 30 minutes to form ink. 100 μL of ink (containing ~2 mg MOF) was spread on the surface of the gas diffusion layer (GDL, 1×1 cm^2) to obtain the working electrode.

Electrochemical measurements were conducted in a three-electrode system (CHI660E, CH Instrument, Shanghai, China) at room temperature. Cyclic voltammetry (CV) scans were conducted in an H-type cell with a three-electrode configuration, which consisted of an Ag/Ag$^+$ (0.01 M AgNO$_3$ in MeCN) reference electrode, a platinum plate electrode as a counter electrode and a working electrode (1×1 cm^2). The electrochemical CO$_2$RR performances of these samples were tested in a catholyte with 0.5 M EmimBF$_4$ in MeCN and an anolyte with 0.5 M H$_2$SO$_4$, using an air-tight H-cell separated by a Nafion 117 proton exchange membrane (CO$_2$-saturated). The experiments were performed in the potential range from −0.6 V to −2.5 V vs. Ag/Ag$^+$ at a potential scan rate of 10 mV s^{-1}. The gas products were quantitatively identified by gas chromatography (GC) and the liquid products were analyzed by ^{1}H nuclear magnetic resonance (^{1}H-NMR) spectra. EIS spectra were recorded at an open-circuit potential of 5.0 mV (10^{-2}–10^5 Hz) using a CO$_2$-saturated electrolyte. Tafel plots were generated from the variation, which was obtained via step potential electrolysis at the partial current density against the applied over-potential.

FE calculations

$$\text{FE}_{\text{gas}} = \frac{Z \times F \times V(\text{mL min}^{-1}) \times v(\text{vol}\%) \times P}{T \times R \times I_{\text{total}} \times 60(\text{s min}^{-1})} \quad (1)$$

where F is the Faraday constant (96 485 C mol^{-1}), Z is the electron transfer number, V is the gas flow rate obtained using a flow meter (10 ml min^{-1}), P is one atmosphere (1.013×10^5 Pa), R is the universal gas constant (8.314 J mol^{-1} K^{-1}), I is the total steady-state cell current, and T is the room temperature (298.15 K).

$$\text{FE}_{\text{HCOOH}} = \frac{Z \times F \times n_{\text{products}}}{Q} \times 100\% \quad (2)$$

where Q denotes the total charge (C) and n_{products} denotes the moles of the obtained formate calculated by ^{1}H-NMR.

Turnover frequency (TOF)

The turnover frequency (TOF) describes the level of catalytic activity and the calculation formula is expressed as below:

$$\text{TOF} = \frac{j_{\text{products}} \times \text{FE}}{Z \times F \times n} \times 3600 \quad (3)$$

where FE is the Faraday efficiency of the product, n is the molar weight of the catalytic sites, and j_{products} is the current density.

Electrochemical surface area (ECSA)

The electrochemical surface area can be used to calculate the number of electrochemically active sites of the electrode, which can be calculated as follows:

$$\text{ECSA} = \frac{C_{\text{dl}}}{C_{\text{s}}} \quad (4)$$

where C_{dl} is the double-layer capacitance obtained by cyclic voltammetric stripping at different scanning rates in the non-Faraday region and C_{s} is the specific capacitance of the corresponding smooth metal or oxide electrode. The slope of the linearity between j and v, $C_{\text{dl}} = j/v$. CV curves from −0.60 V to −0.65 V vs. Ag/Ag$^+$ were measured at different scan rates, and then the electrochemical surface area was calculated.

DFT calculations

We performed the DFT calculations using the Quantum-ESPRESSO package as implemented in the PWscf code.[44] The projector augmented wave pseudopotentials were used to describe the interactions between the valence electrons and ionic cores.[45] We used 50 and 500 Ry cutoffs for the kinetic energy of the plane-wave basis and charge density, respectively. The Perdew–Burke–Ernzerhof form of the generalized gradient approximation was employed to describe the electronic exchange and correlation.[46] For simplification, the trinuclear metal clusters (In$_3$-cluster and InCo$_2$-cluster) with eight-coordinated ligands, which were simplified from the experimental single-crystal structure, were used for DFT calculations.

Results and discussion

Material characterization

Single-crystal X-ray diffraction analysis (Tables S1 and S2†) reveals that InCo-ABDBC-HIN crystallizes in the $I\bar{4}3d$ space group. Its asymmetric structure contains a half μ$_3$-OH, one half indium atom, one cobalt atom, one ABDBC ligand, one HIN ligand and one coordination hydrone (Fig. S5†). Both Co^{2+} ions of the InCo$_2$O cluster exhibit six-coordination by one μ$_3$-OH, four O atoms and one N atom. [InCo$_2$(μ$_3$-OH)(O$_2$C)$_6$(H$_2$O)(py)$_2$] is surrounded by one coordination hydrone, two pyridyl groups of HIN, two –COO$^-$ from HIN and four –COO$^-$ from H$_2$ABDBC ligands (Fig. 1a). Interestingly, only two apical sites are occupied by HIN ligands and the third one is coordinated by a hydrone in the trinuclear cluster, which provides active sites for the interaction between adsorbents and the host framework (Fig. 1b). An SEM image shows that InCo-ABDBC-HIN exhibits an irregular 3D polyhedron structure (Fig. S6†).

The X-ray diffraction (XRD) results of the samples are basically consistent with the simulation results, indicating the successful synthesis of the target MOFs. The XRD patterns of InCo-ABDBC-HIN are consistent with that of In-ABDBC-HIN, indicating that the entire framework has not changed after the introduction of Co (Fig. 2a). ICP-MS (Fig. S7†) suggests that the atomic ratio of In : Co in InCo-ABDBC-HIN is approxi-

160 | *Inorg. Chem. Front.*, 2023, **10**, 158–167

This journal is © the Partner Organisations 2023
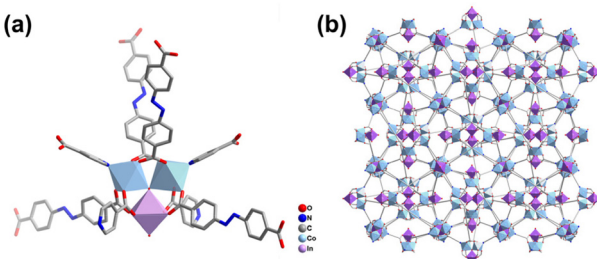
Fig. 1 (a) Structure of the coordination environment of the metal atom and (b) the 3D framework structure along the *a*-axis.
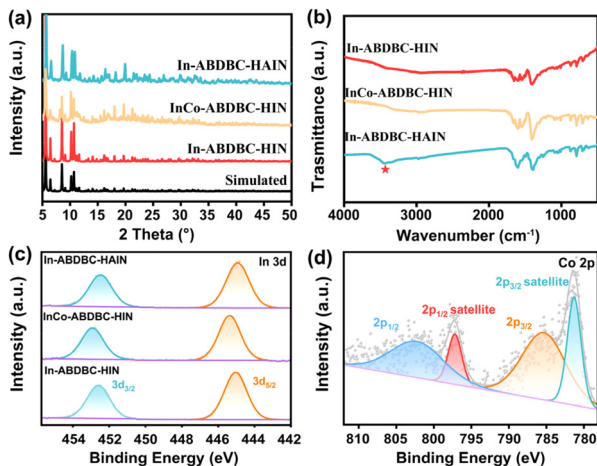
Fig. 2 (a) XRD patterns, (b) FTIR spectra and (c) In 3d XPS spectra for In-ABDBC-HIN, InCo-ABDBC-HIN and In-ABDBC-HAIN. (d) Co 2p XPS spectra of InCo-ABDBC-HIN.

mately 1 : 1.6, which is close to the theoretical value based on the single-crystal structure. In FT-IR, the peak at 3449 cm^{-1} is due to the antisymmetric stretching modes of the amino group, suggesting the successful introduction of the amino group (Fig. 2b). TGA curves (Fig. S8†) show that a series of single indium site MOF frameworks can remain stable up to about 370 °C, implying that these In-based MOFs are thermally robust.

The electronic structures of In-ABDBC-HIN, InCo-ABDBC-HIN, and In-ABDBC-HAIN were further employed for X-ray photoelectron spectroscopy (XPS). All the resulting XPS spectra were calibrated with the C (sp^2) peak position at 284.6 eV in the C 1s spectra (Fig. S9†). The peak of In 3d (445 eV/452 eV) indicates that In^{3+} species dominate (Fig. 2c).[47] For InCo-ABDBC-HIN, due to the effects of Co, the binding energies of both In 3d$_{5/2}$ and In 3d$_{3/2}$ are left shifted (Fig. 2c). The above results imply that the replacement of In by Co atoms alters the entire electronic structure of the active sites in InCo-ABDBC-HIN.[48] The peak profile of Co 2p (445 eV/452 eV) indicates the existence of Co^{2+} species in InCo-ABDBC-HIN (Fig. 2d).[49] The charge difference between the In ions and Co ions modifies the charge distribution in the InCo$_2$-cluster,

which is promising to enhance both the CO$_2$ adsorption capacity and the electrocatalytic CO$_2$RR performance.

Carbon dioxide capture. CO$_2$ adsorption isotherms of activated In-MOF materials were investigated to determine the effect of a polymetallic strategy on the porous environments of MOFs. N$_2$ adsorption–desorption isotherms at 77 K were first profiled to reveal the pore structure of these samples. As shown in Fig. 3a, nitrogen sorption curves show completely reversible type-I isotherms, representative of the microporous structure of the samples. In addition, the Brunauer–Emmett–Teller (BET) surface areas of In-ABDBC-HIN, InCo-ABDBC-HIN, and In-ABDBC-HAIN are 958, 1355, and 1106 m^2 g^{-1}, respectively, which shows that the introduction of cobalt and the functional groups greatly increased the specific surface area (SSA). Based on the N$_2$ adsorption–desorption isotherm, the pore size distribution of the samples was calculated using the Horvath–Kawazoe model, which suggested that the pore sizes are mainly in the range 0.6–0.8 nm for these samples (Fig. S10†).

The CO$_2$ uptake performance under both low pressure and high pressure was further studied. (Fig. 3b, c and Fig. S11, 12†). The maximum CO$_2$ uptakes of In-ABDBC-HIN, InCo-ABDBC-HIN, and In-ABDBC-HAIN under low pressure at 273 K are 68.5, 101.7, and 94.8 cm^3 g^{-1}, respectively. In-ABDBC-HAIN shows higher CO$_2$ uptake than In-ABDBC-HIN, implying that the amine functionalization can enhance the CO$_2$ uptake ability.[50] InCo-ABDBC-HIN shows the highest CO$_2$ uptake capacity, suggesting that the incorporated Co is efficient to promote the gas uptake ability due to the modified electronic structure. For high-pressure CO$_2$ adsorption (Fig. 3c), due to the fact that the effect of amino modification on the adsorption of CO$_2$ molecules is greater than that of Co replacement, the maximum CO$_2$ uptakes of In-ABDBC-HIN, InCo-
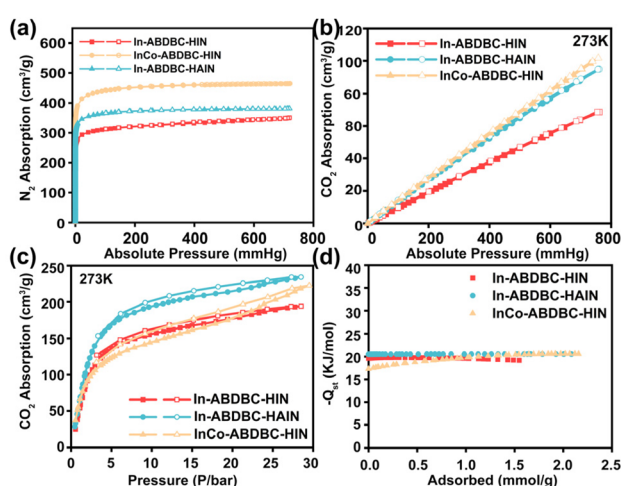
Fig. 3 (a) N$_2$ adsorption and desorption isotherms at 77 K, (b) low-pressure CO$_2$ adsorption isotherms at 273 K and (c) high-pressure CO$_2$ adsorption isotherms at 273 K for In-ABDBC-HIN, InCo-ABDBC-HIN, and In-ABDBC-HAIN. (d) Isosteric heat of adsorption (Q_{st}).

This journal is © the Partner Organisations 2023

Inorg. Chem. Front., 2023, **10**, 158–167 | **161**

ABDBC-HIN, and In-ABDBC-HAIN at 273 K are 193.9, 222.6, and 234.2 cm^3 g^{-1}, respectively.

To determine the interaction between the CO_2 molecules and these In-MOF materials, the virial model was used to analyze the isosteric adsorption enthalpy (Q_{st}) (Fig. 3d). The enthalpy of adsorption at zero-coverage $\left(Q_{st}^{\circ}\right)$ values on In-ABDBC-HIN, InCo-ABDBC-HIN, and In-ABDBC-HAIN were 19.6, 17.3, and 20.4 kJ mol^{-1}, respectively, indicating that the interaction between the MOF skeleton and the CO_2 molecules is weaker because of the incorporation of Co, and skeleton charge is the main factor affecting the CO_2 adsorption performance, which is in good agreement with the XPS spectra. The results of CO_2 uptake performance demonstrate the great potential of InCo-ABDBC-HIN for efficient CO_2 conversion.

Electrochemical CO_2 reduction. The electrochemical CO_2RR performances of these samples were tested in a catholyte with 0.5 M EmimBF$_4$ in MeCN and an anolyte with 0.5 M H_2SO_4, using an air-tight H-cell separated by a Nafion-117 proton exchange membrane (CO_2-saturated).[51] A gas diffusion layer (GDL) with a coarse surface was used as the support to fabricate the working electrodes. The potentials mentioned in this work are all related to Ag/Ag$^+$ and there is no IR compensation.

The cyclic voltammetry curve of InCo-ABDBC-HIN was plotted to determine its electrocatalytic activity for the CO_2RR (Fig. S13†). Obviously, the current density is higher in the CO_2-saturated electrolyte than in the Ar-saturated electrolyte, especially as the voltage is lower than −1.5 V, suggesting that their activities resulted from the CO_2RR. The potential range for the electrochemical CO_2RR was from −2 to −2.4 V vs. Ag/Ag$^+$. Fig. 4a shows the representative linear scanning voltammetry (LSV) curves of In-ABDBC-HIN, InCo-ABDBC-HIN, and In-ABDBC-HAIN. The current density from high to low is: InCo-ABDBDC-HIN > In-ABDBC-HIN > In-ABDBC-HAIN in the CO_2-saturated electrolyte, indicating that metal substitution is

beneficial for the improvement of catalytic activity, while the modification of functional groups in ligands reduces the CO_2RR activity.

Electrolysis was performed at a given potential to further determine their reduction products. The gas products were quantitatively identified by GC (Fig. S14†) and the liquid products were analyzed by ^{1}H-NMR spectra (Fig. S15†). The electrocatalytic process continued for 1 hour and the results are summarized in Fig. 4b and c. As the applied potential increases, the current density correspondingly increases (Fig. S16†). The FE for all three samples reached the maximum at −2.2 V vs. Ag/Ag$^+$. Fig. 4b compares the FE for various catalysts at various potentials. In-ABDBC-HIN shows a higher current density than In-ABDBC-HAIN at −2.2 V vs. Ag/Ag$^+$ (Fig. 4c), indicating that the amino functional groups in In-ABDBC-HAIN are not conducive to the catalytic capability, which conflicts with the results on CO_2 adsorption tests and the conclusion in some of the previous work.[36] We further measured the CO_2RR activity of InCo-ABDBC-HAIN to study the effects of amino modification. As shown in Fig. S17,† compared with InCo-ABDBC-HIN, InCo-ABDBC-HAIN shows reduced CO_2RR performance. The above results suggest that amino modification reduces the activity for the CO_2RR. We infer that the poor performance of In-ABDBC-HAIN is attributed to the increased steric hindrance caused by the amino modification that prevents CO_2 molecules from approaching the catalytic site. The subsequent DFT calculations suggest that the amino modification suppresses the electrical conductivity, which may be a major factor for the poor CO_2RR activity of the HAIN-modified samples. Among all samples, InCo-ABDBC-HIN exhibits the highest electrocatalytic activity for the CO_2RR. The FE of C_1 products (FE_{C_1}) reaches 81.5% with a current density of 21.20 mA cm^{-2} under a potential of −2.2 V vs. Ag/Ag$^+$ for InCo-ABDBC-HIN, suggesting that the incorpor-
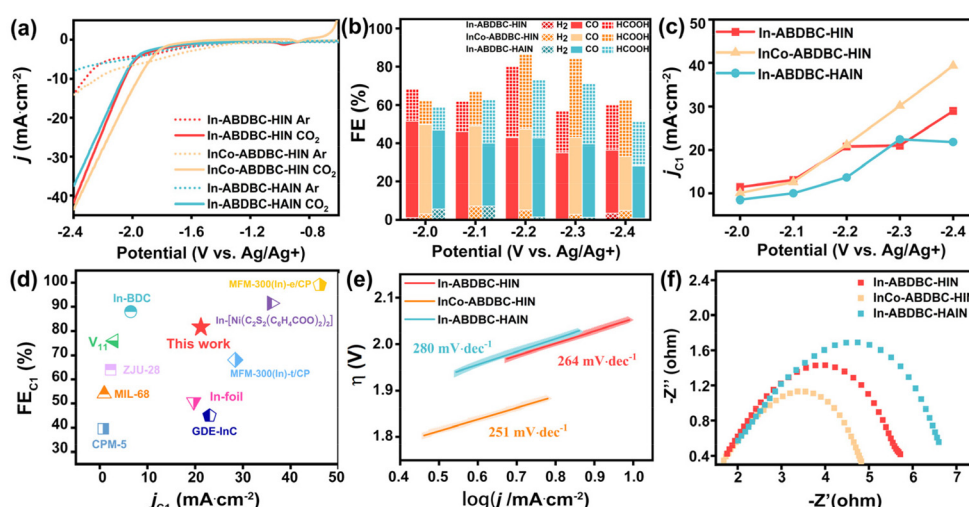
Fig. 4 (a) LSV curves, (b) FE and (c) current densities at different operation voltages of In-ABDBC-HIN, InCo-ABDBC-HIN and In-ABDBC-HAIN. (d) Comparison of InCo-ABDBC-HIN performance with other indium-based catalysts. (e) Tafel slopes and (f) Nyquist plots of In-ABDBC-HIN, InCo-ABDBC-HIN, and In-ABDBC-HAIN.

162 | *Inorg. Chem. Front.*, 2023, **10**, 158–167

This journal is © the Partner Organisations 2023

ation of Co into the framework greatly enhanced the electrocatalytic performance. Moreover, we calculated the turnover frequency (TOF, Fig. S18†) of these samples and also found that the catalytic performance of InCo-ABDBC-HIN exceeds that of In-ABDBC-HIN and In-ABDBC-HAIN when the potential is <−2.2 V vs. Ag/Ag$^+$. The electrochemical surface area (ECSA) of InCo-ABDBC-HIN exhibited a slightly larger C_{dl} (72 mF cm^{-2}) value than In-ABDBC-HIN (63 mF cm^{-2}) and In-ABDBC-HAIN (60 mF cm^{-2}) (Fig. S19†). The very small difference in the ECSA implies that the high activity of InCo-ABDBC-HIN is mainly attributed to the high intrinsic activity resulting from the incorporation of Co atoms. The bimetal InCo cluster modified the electronic structure and promoted the adsorption of CO_2 and the activation of CO_2, thereby leading to superior electrocatalytic CO_2RR activity. Fig. 4d shows that the CO_2RR activity of InCo-ABDBC-HIN is superior to most of the MOF-based catalysts (Table S3†).

To research the kinetics of CO_2 reduction to C_1 products over different electrocatalysts, the Tafel slope was measured (Fig. 4e). The resulting Tafel slope of InCo-ABDBC-HIN was 251 mV dec^{-1}, which is smaller than that of In-ABDBC-HIN (264 mV dec^{-1}) and In-ABDBC-HAIN (280 mV dec^{-1}), implying the fast charge transfer in InCo-ABDBC-HIN. The production of OCHO* or *COOH is a rate-controlling step, which is formed by adsorbed carbon dioxide accepting an electron and binding to H$^+$ in the electrolyte.[10,52,53] The kinetics of the electrode/electrolyte interface in the electrocatalytic CO_2 process is represented by electrochemical impedance spectroscopy (EIS). The Nyquist plot diagram shows that the charge transfer resistance (R_{ct}) of InCo-ABDBC-HIN (3.24 Ω) is significantly lower than that of In-ABDBC-HIN (3.94 Ω) and In-ABDBC-HIN (4.59 Ω), indicating that the charge transfer kinetics of InCo-ABDBC-HIN is the fastest (Fig. 4f).

Long-term durability and cycling reproducibility were further studied to show the stability of InCo-ABDBC-HIN. The catalyst was subjected to the electrocatalytic CO_2RR for con-

secutive 12 hours at −2.2 V vs. Ag/Ag$^+$ to evaluate long-term durability (Fig. 5a). Although there was a slightly decrease in FE$_{C1}$, the current density of InCo-ABDBC-HIN was maintained at 26.5 mA cm^{-2}, indicating the high continuous durability. The repeatability of the In-MOF was demonstrated by five times successive repeatability tests (Fig. 5b). The FE$_{C1}$ retention after five times cyclic reuse reaches as high as 83.6%. The XRD patterns after long-term electrolysis show that the structure has been well preserved, implying high structural stability (Fig. 5c). In the N 1s XPS spectra after electrolysis with the InCo-ABDBC-HIN catalyst, an additional peak was observed at 401.7 eV (Fig. 5d), which was due to the N element in the electrolyte.[54] In 3d is slightly shifted to a low binding energy as part of In^{3+} is reduced to In^0 during the electroreduction of CO_2 (Fig. 5e).[55] The Co 2p XPS spectra of the InCo-ABDBC-HIN catalyst did not change obviously before and after electrolysis (Fig. 5f). ICP-MS suggests that after continuous electrocatalysis, In and Co metals were slightly dissolved into the electrolyte, which is responsible for the reduced activity (Fig. S20†).[56] All these results demonstrate that the obtained InCo-ABDBC-HIN is an efficient and stable catalyst for the CO_2RR.

DFT calculations. To reveal the effects of bimetal engineering and amino functionalization on the electronic structure, DFT theoretical calculations were further performed on In-ABDBC-HIN, In-ABDBC-HAIN, and InCo-ABDBC-HIN, which were simplified from the experimental single-crystal structures (Fig. 6a–c and Fig. S21†). As shown in Fig. 6a and b, no unpaired electronic distribution can be observed on metal atoms in both In-ABDBC-HIN and In-ABDBC-HAIN. Fig. 6a and b also imply that the amino modification nearly does not affect the charge distribution on the In$_3$-cluster. After the incorporation of Co into the In$_3$-cluster (Fig. 6c), InCo-ABDBC-HIN exhibits an obvious unpaired electronic distribution on Co metals. These unpaired electrons are promising for participating in the CO_2RR, leading to the enhanced activity for the CO_2RR. Fig. 6d shows that the DOS intensity at
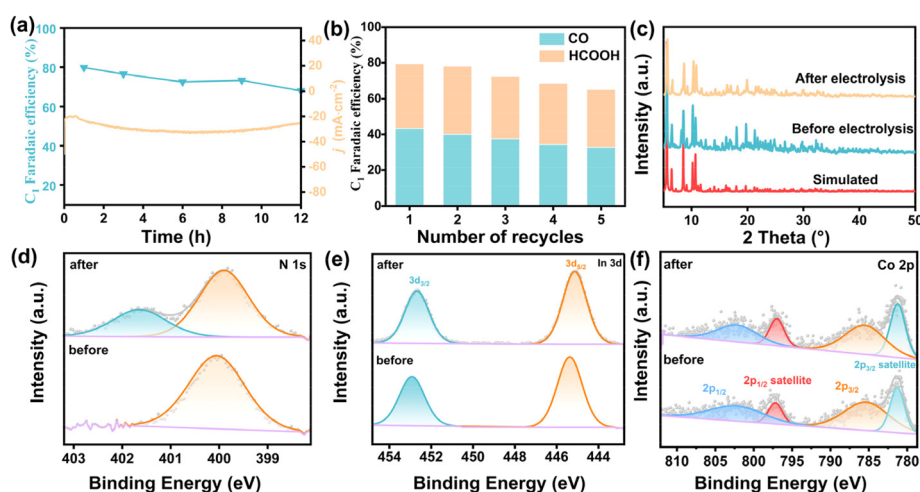
Fig. 5 (a) Long-term durability of InCo-ABDBC-HIN. (b) FE after five times electrolysis at −2.2 V vs. Ag/Ag$^+$. (c) Comparison of XRD spectra, (d) N 1s, (e) In 3d and (f) Co 2p XPS of InCo-ABDBC-HIN before and after electrolysis.
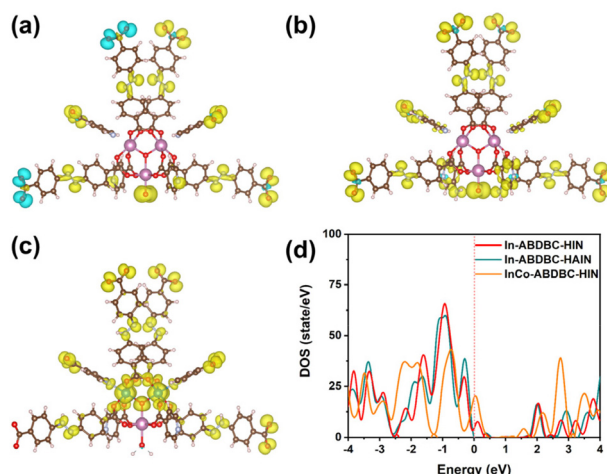
Fig. 6 The distribution of unpaired electrons in (a) In-ABDBC-HIN, (b) In-ABDBC-HAIN, and (c) InCo-ABDBC-HIN. (d) DOS of In-ABDBC-HIN, In-ABDBC-HAIN, and InCo-ABDBC-HIN. The pink dotted line represents the location of the Fermi energy.

the Fermi energy level of InCo-ABDBC-HIN is improved compared with that of the other two structures, implying that the substitution of Co improves the electrical conductivity.[57,58] Moreover, the DOS intensity at the Fermi energy level of In-ABDBC-HAIN is extremely poor, indicating that the electrical conductivity is greatly suppressed due to the introduction of HAIN, thereby leading to the poor CO_2RR activity. Overall, InCo-ABDBC-HIN demonstrates improved unpaired electronic distribution and enhanced electrical conductivity, and improves the CO_2RR activity.

Conclusions

In summary, we report a unique trinuclear cluster In-based MOF for efficient CO_2 capture and the electrocatalytic CO_2RR. The precise structural control *via* bimetal engineering and ligand modification was carried out to optimize the activity. Due to the modified electronic structure and surface charge modification, InCo-ABDBC-HIN, in which In atoms are partially substituted by Co, demonstrates the highest CO_2 uptake performance and CO_2RR activity among all the investigated samples. The CO_2 uptake capacity at 273 K under low pressure and high pressure is 101.7 and 222.6 cm^3 g^{-1}, respectively. The current density under a potential of −2.2 V *vs*. Ag/Ag$^+$ reaches up to 21.2 mA cm^{-2}, while a high FE_{C1} of 81.5% is achieved. InCo-ABDBC-HIN also shows high long-term stability, good durability, and structural immobility during electrocatalysis. DFT calculations suggest that the substitution of In by Co significantly modified the electronic structure of In-based clusters, which provides rich unpaired electrons for the CO_2RR and enhances the charge transfer efficiency. Our work demonstrated a novel trinuclear indium cluster-based MOF for efficient CO_2 capture and electrocatalytic conversion.

Author contributions

Shuo Wang: methodology, data collection, and writing original draft. Ying Wang: writing original draft. Jia-Min Huo: data analysis. Wen-Yu Yuan: supervision, writing, checking & editing. Peng Zhang: data analysis – single-crystal analysis. Shu-Ni Li: investigation and resources. Quan-Guo Zhai: conceptualization, supervision, and funding acquisition.

Conflicts of interest

There are no conflicts to declare.

Acknowledgements

References

1 L. Li, Y. Huang and Y. Li, Carbonaceous materials for electrochemical CO_2 reduction, *Energy Chem.*, 2020, **2**, 100024.

2 K. j. Puring, O. Evers, M. Prokein, D. Siegmund, F. Scholten, N. Mölders, M. Renner, B. R. Cuenya, M. Petermann, E. Weidner and U.-P. Apfel, Assessing the Influence of Supercritical Carbon Dioxide on the Electrochemical Reduction to Formic Acid Using Carbon-Supported Copper Catalysts, *ACS Catal.*, 2020, **10**, 12783–12789.

3 G. R. Zhang, S. D. Straub, L. L. Shen, Y. Hermans, P. Schmatz, A. M. Reichert, J. P. Hofmann, I. Katsounaros and B. J. M. Etzold, Probing CO_2 Reduction Pathways for Copper Catalysis Using an Ionic Liquid as a Chemical Trapping Agent, *Angew. Chem., Int. Ed.*, 2020, **59**, 18095–18102.

4 S. Sinha, R. Zhang and J. J. Warren, Low Overpotential CO_2 Activation by a Graphite-Adsorbed Cobalt Porphyrin, *ACS Catal.*, 2020, **10**, 12284–12291.

5 J. Zeng, M. R. Fiorentin, M. Fontana, M. Castellino, F. Risplendi, A. Sacco, G. Cicero, M. A. Farkhondehfal, F. Drago and C. F. Pirri, Novel Insights into Sb-Cu Catalysts for Electrochemical Reduction of CO_2, *Appl. Catal., B*, 2022, **306**, 121089.

6 R. Zhao, P. Ding, P. Wei, L. Zhang, Q. Liu, Y. Luo, T. Li, S. Lu, X. Shi, S. Gao, A. M. Asiri, Z. Wang and X. Sun,

164 | *Inorg. Chem. Front.*, 2023, **10**, 158–167

This journal is © the Partner Organisations 2023

Recent Progress in Electrocatalytic Methanation of CO_2 at Ambient Conditions, *Adv. Funct. Mater.*, 2021, **31**, 2009449.

7 R. Cao, J. D. Yi, R. Xie, Z. L. Xie, G. L. Chai, T. F. Liu, R. P. Chen and Y. B. Huang, Highly Selective CO_2 Electroreduction to CH_4 by in situ Generated Cu_2O Single-Type Sites on Conductive MOF: Stabilizing Key Intermediates with Hydrogen Bond, *Angew. Chem., Int. Ed.*, 2020, **59**, 23641–23648.

8 Y. Liu, S. Li, L. Dai, J. Li, J. Lv, Z. Zhu, A. Yin, P. Li and B. Wang, The Synthesis of Hexaazatrinaphthylene-Based 2D Conjugated Copper Metal-Organic Framework for Highly Selective and Stable Electroreduction of CO_2 to Methane, *Angew. Chem., Int. Ed.*, 2021, **60**, 16409–16415.

9 D. Xu, Y. Xu, H. Wang and X. Qiu, Highly efficient and stable indium single-atom catalysts for electrocatalytic reduction of CO_2 to formate, *Chem. Commun.*, 2022, **58**, 3007–3010.

10 P. Lu, D. Gao, H. He, Q. Wang, Z. Liu, S. Dipazir, M. Yuan, W. Zu and G. Zhang, Facile synthesis of a bismuth nano-structure with enhanced selectivity for electrochemical conversion of CO_2 to formate, *Nanoscale*, 2019, **11**, 7805–7812.

11 H. Luo, B. Li, J. G. Ma and P. Cheng, Surface Modification of Nano-Cu_2O for Controlling CO_2 Electrochemical Reduction to Ethylene and Syngas, *Angew. Chem., Int. Ed.*, 2022, **61**, e202116736.

12 H. Sun, L. Chen, L. Xiong, K. Feng, Y. Chen, X. Zhang, X. Yuan, B. Yang, Z. Deng, Y. Liu, M. H. Rummeli, J. Zhong, Y. Jiao and Y. Peng, Promoting ethylene production over a wide potential window on Cu crystallites induced and stabilized via current shock and charge delocalization, *Nat. Commun.*, 2021, **12**, 6823.

13 D. H. Nam, O. S. Bushuyev, J. Li, P. De Luna, A. Seifitokaldani, C. T. Dinh, F. P. G. de Arquer, Y. H. Wang, Z. Q. Liang, A. H. Proppe, C. S. Tan, P. Todorovic, O. Shekhah, C. M. Gabardo, J. W. Jo, J. M. Choi, M. J. Choi, S. W. Baek, J. Kim, D. Sinton, S. O. Kelley, M. Eddaoudi and E. H. Sargent, Metal-Organic Frameworks Mediate Cu Coordination for Selective CO_2 Electroreduction, *J. Am. Chem. Soc.*, 2018, **140**, 11378–11386.

14 Y. Y. Zhang, K. Li, M. M. Chen, J. Wang, J. D. Liu and Y. T. Zhang, Cu/Cu_2O Nanoparticles Supported on Vertically ZIF-L-Coated Nitrogen-Doped Graphene Nanosheets for Electroreduction of CO_2 to Ethanol, *ACS Appl. Nano Mater.*, 2020, **3**, 257–263.

15 H. Huo, J. Wang, Q. Fan, Y. Hu and J. Yang, Cu–MOFs Derived Porous Cu Nanoribbons with Strengthened Electric Filed for Selective CO_2 Electroreduction to C^{2+} Fuels, *Adv. Energy Mater.*, 2021, **11**, 2102447.

16 H. Q. Liang, T. Beweries, R. Francke and M. Beller, Molecular Catalysts for Reductive Homocoupling of CO_2 towards C^{2+} Compounds, *Angew. Chem., Int. Ed.*, 2022, **61**, e202116736.

17 F. Yang, W. Fang, Q. Wang, P. Deng and B. Y. Xia, Optimizing Copper Oxidation State to Promote Ethylene Generation in Efficient Carbon Dioxide Conversion, *ACS Sustainable Chem. Eng.*, 2022, **10**, 4677–4682.

18 H. G. Zhang, J. Z. Li, Q. Tan, L. L. Lu, Z. B. Wang and G. Wu, Metal-Organic Frameworks and Their Derived Materials as Electrocatalysts and Photocatalysts for CO_2 Reduction: Progress, Challenges, and Perspectives, *Chem. – Eur. J.*, 2018, **24**, 18137–18157.

19 W. Yuan, Y. Ma, H. Wu and L. Cheng, Single-atom catalysts for CO oxidation, CO_2 reduction, and O_2 electrochemistry, *J. Energy Chem.*, 2022, **65**, 254–279.

20 J. Liu, P. K. Thallapally, B. P. McGrail, D. R. Brown and J. Liu, Progress in adsorption-based CO_2 capture by metal–organic frameworks, *Chem. Soc. Rev.*, 2012, **41**, 2308–2322.

21 Y. Y. Birdja, E. Pérez-Gallent, M. C. Figueiredo, A. J. Göttle, F. Calle-Vallejo and M. T. M. Koper, Advances and challenges in understanding the electrocatalytic conversion of carbon dioxide to fuels, *Nat. Energy*, 2019, **4**, 732–745.

22 F. M. Li, L. Huang, S. Zaman, W. Guo, H. Liu, X. Guo and B. Y. Xia, Corrosion Chemistry of Electrocatalysts, *Adv. Mater.*, 2022, e2200840.

23 P. Lamagni, M. Miola, J. Catalano, M. S. Hvid, M. A. H. Mamakhel, M. Christensen, M. R. Madsen, H. S. Jeppesen, X. M. Hu, K. Daasbjerg, T. Skrydstrup and N. Lock, Restructuring Metal–Organic Frameworks to Nanoscale Bismuth Electrocatalysts for Highly Active and Selective CO_2 Reduction to Formate, *Adv. Funct. Mater.*, 2020, **30**, 1910408.

24 L. Sun, V. Reddu, A. C. Fisher and X. Wang, Electrocatalytic reduction of carbon dioxide: opportunities with hetero-geneous molecular catalysts, *Energy Environ. Sci.*, 2020, **13**, 374–403.

25 X. Feng, Y. Pi, Y. Song, C. Brzezinski, Z. Xu, Z. Li and W. Lin, Metal-Organic Frameworks Significantly Enhance Photocatalytic Hydrogen Evolution and CO_2 Reduction with Earth-Abundant Copper Photosensitizers, *J. Am. Chem. Soc.*, 2020, **142**, 690–695.

26 Y. Zhang, X. L. Zhang, Y. L. Zhu, B. B. Qian, A. M. Bond and J. Zhang, The Origin of the Electrocatalytic Activity for CO_2 Reduction Associated with Metal-Organic Frameworks, *ChemSusChem*, 2020, **13**, 2552–2556.

27 X. Kang, Q. Zhu, X. Sun, J. Hu, J. Zhang, Z. Liu and B. Han, Highly efficient electrochemical reduction of CO_2 to CH_4 in an ionic liquid using a metal-organic framework cathode, *Chem. Sci.*, 2016, **7**, 266–273.

28 P. Shao, L. Yi, S. Chen, T. Zhou and J. Zhang, Metal-organic frameworks for electrochemical reduction of carbon dioxide: The role of metal centers, *J. Energy Chem.*, 2020, **40**, 156–170.

29 K. Lei and B. Y. Xia, Electrocatalytic CO_2 Reduction: from Discrete Molecular Catalysts to Their Integrated Catalytic Materials, *Chem. – Eur. J.*, 2022, **28**, e202200141.

30 Y. Bochlin, L. Ezuz, Y. Kadosh, D. Benjamin, Y. Mordekovitz, S. Hayun, E. Korin and A. Bettelheim, Enhancement of Electrocatalytic CO_2 Reduction to Methane by CoTMPyP when Hosted in a 3D Covalent Graphene Framework, *ACS Appl. Energy Mater.*, 2021, **4**, 10033–10041.

This journal is © the Partner Organisations 2023

Inorg. Chem. Front., 2023, **10**, 158–167 | **165**

31 M. Abdinejad, C. Dao, X.-A. Zhang and H. B. Kraatz, Enhanced electrocatalytic activity of iron amino porphyrins using a flow cell for reduction of CO_2 to CO, *J. Energy Chem.*, 2021, **58**, 162–169.

32 Ö. Durak, H. Kulak, S. Kavak, H. M. Polat, S. Keskin and A. Uzun, Towards complete elucidation of structural factors controlling thermal stability of IL/MOF composites: Effects of ligand functionalization on MOFs, *J. Phys.: Condens. Matter*, 2020, **32**, 484001.

33 A. Zhang, Y. Liang, H. Li, B. Zhang, Z. Liu, Q. Chang, H. Zhang, C. F. Zhu, Z. Geng, W. Zhu and J. Zeng, In-Situ Surface Reconstruction of InN Nanosheets for Efficient CO_2 Electroreduction into Formate, *Nano Lett.*, 2020, **20**, 8229–8235.

34 Z. Chen, X. Zhang, M. Jiao, K. Mou, X. Zhang and L. Liu, Engineering Electronic Structure of Stannous Sulfide by Amino–Functionalized Carbon: Toward Efficient Electrocatalytic Reduction of CO_2 to Formate, *Adv. Energy Mater.*, 2020, **10**, 1903664.

35 Y. Zhou, S. Liu, Y. Gu, G. H. Wen, J. Ma, J. L. Zuo and M. Ding, In(III) Metal-Organic Framework Incorporated with Enzyme-Mimicking Nickel Bis(dithiolene) Ligand for Highly Selective CO_2 Electroreduction, *J. Am. Chem. Soc.*, 2021, **143**, 14071–14076.

36 Z. Wang, Y. Zhou, C. Xia, W. Guo, B. You and B. Y. Xia, Efficient Electroconversion of Carbon Dioxide to Formate by a Reconstructed Amino-Functionalized Indium-Organic Framework Electrocatalyst, *Angew. Chem., Int. Ed.*, 2021, **60**, 19107–19112.

37 S. Rasul, D. H. Anjum, A. Jedidi, Y. Minenkov, L. Cavallo and K. Takanabe, A highly selective copper-indium bimetallic electrocatalyst for the electrochemical reduction of aqueous CO_2 to CO, *Angew. Chem., Int. Ed.*, 2015, **54**, 2146–2150.

38 Y. Sun, B. Xia, S. Ding, L. Yu, S. Chen and J. Duan, Rigid two-dimensional indium metal–organic frameworks boosting nitrogen electroreduction at all pH values, *J. Mater. Chem. A*, 2021, **9**, 20040–20047.

39 A. Pustovarenko, A. Dikhtiarenko, A. Bavykina, L. Gevers, A. Ramírez, A. Russkikh, S. Telalovic, A. Aguilar, J.-L. Hazemann, S. Ould-Chikh and J. Gascon, Metal–Organic Framework-Derived Synthesis of Cobalt Indium Catalysts for the Hydrogenation of CO_2 to Methanol, *ACS Catal.*, 2020, **10**, 5064–5076.

40 X. Jiang, R. Fan, X. Zhou, K. Zhu, T. Sun, X. Zheng, K. Xing, W. Chen and Y. Yang, Mixed functionalization strategy on indium-organic framework for multiple ion detection and H_2O_2 turn-on sensing, *Dalton Trans.*, 2021, **50**, 7554–7562.

41 S. C. Fan, S. Q. Chen, J. W. Wang, Y. P. Li, P. Zhang, Y. Wang, W. Yuan and Q. G. Zhai, Precise Introduction of Single Vanadium Site into Indium-Organic Framework for CO_2 Capture and Photocatalytic Fixation, *Inorg. Chem.*, 2022, **61**, 14131–14139.

42 C. C. Epley, M. D. Love and A. J. Morris, Characterizing Defects in a UiO-AZB Metal-Organic Framework, *Inorg. Chem.*, 2017, **56**, 13777–13784.

43 X. Gu, Z. H. Lu and Q. Xu, High-connected mesoporous metal-organic framework, *Chem. Commun.*, 2010, **46**, 7400–7402.

44 P. Giannozzi, S. Baroni, N. Bonini, M. Calandra, R. Car, C. Cavazzoni, D. Ceresoli, G. L. Chiarotti, M. Cococcioni, I. Dabo, A. Dal Corso, S. de Gironcoli, S. Fabris, G. Fratesi, R. Gebauer, U. Gerstmann, C. Gougoussis, A. Kokalj, M. Lazzeri, L. Martin-Samos, N. Marzari, F. Mauri, R. Mazzarello, S. Paolini, A. Pasquarello, L. Paulatto, C. Sbraccia, S. Scandolo, G. Sclauzero, A. P. Seitsonen, A. Smogunov, P. Umari and R. M. Wentzcovitch, QUANTUM ESPRESSO: a modular and open-source software project for quantum simulations of materials, *J. Phys.: Condens. Matter*, 2009, **21**, 395502.

45 P. E. Blochl, Projector augmented-wave method, *Phys. Rev. B: Condens. Matter Mater. Phys*, 1994, **50**, 17953–17979.

46 K. B. John, P. Perdew and M. Ernzerhof, Generalized Gradient Approximation Made Simple, *Phys. Rev. Lett.*, 1996, **77**, 3865–3868.

47 S. Z. Hou, X. D. Zhang, W. W. Yuan, Y. X. Li and Z. Y. Gu, Indium-Based Metal-Organic Framework for High-Performance Electroreduction of CO_2 to Formate, *Inorg. Chem.*, 2020, **59**, 11298–11304.

48 G. Wen, D. U. Lee, B. Ren, F. M. Hassan, G. Jiang, Z. P. Cano, J. Gostick, E. Croiset, Z. Bai, L. Yang and Z. Chen, Orbital Interactions in Bi-Sn Bimetallic Electrocatalysts for Highly Selective Electrochemical CO_2 Reduction toward Formate Production, *Adv. Energy Mater.*, 2018, **8**, 1802427.

49 Q. Huang, Q. Li, J. Liu, Y. R. Wang, R. Wang, L. Z. Dong, Y. H. Xia, J. L. Wang and Y.-Q. Lan, Disclosing CO_2 Activation Mechanism by Hydroxyl-Induced Crystalline Structure Transformation in Electrocatalytic Process, *Matter*, 2019, **1**, 1656–1668.

50 X. Li and Q.-L. Zhu, MOF-based materials for photo- and electrocatalytic CO_2 reduction, *Energy Chem.*, 2020, **2**, 100033.

51 J. Feng, S. Zeng, H. Liu, J. Feng, H. Gao, L. Bai, H. Dong, S. Zhang and X. Zhang, Insights into Carbon Dioxide Electroreduction in Ionic Liquids: Carbon Dioxide Activation and Selectivity Tailored by Ionic Microhabitat, *ChemSusChem*, 2018, **11**, 3191–3197.

52 J. H. Koh, D. H. Won, T. Eom, N.-K. Kim, K. D. Jung, H. Kim, Y. J. Hwang and B. K. Min, Facile CO_2 Electro-Reduction to Formate via Oxygen Bidentate Intermediate Stabilized by High-Index Planes of Bi Dendrite Catalyst, *ACS Catal.*, 2017, **7**, 5071–5077.

53 N. Han, Y. Wang, H. Yang, J. Deng, J. Wu, Y. Li and Y. Li, Ultrathin bismuth nanosheets from in situ topotactic transformation for selective electrocatalytic CO_2 reduction to formate, *Nat. Commun.*, 2018, **9**, 1320.

54 D. Karapinar, N. T. Huan, N. R. Sahraie, J. Li, D. Wakerley, N. Touati, S. Zanna, D. Taverna, L. H. G. Tizei, A. Zitolo, F. Jaouen, V. Mougel and M. Fontecave, Electroreduction of CO_2 on Single-Site Copper-Nitrogen-Doped Carbon Material: SelectiveFormation of Ethanol and Reversible

Restructuration of the Metal Sites, *Angew. Chem.*, 2019, **131**, 15242–15247.

55 W. Ma, S. Xie, X. G. Zhang, F. Sun, J. Kang, Z. Jiang, Q. Zhang, D. Y. Wu and Y. Wang, Promoting electrocatalytic CO_2 reduction to formate via sulfur-boosting water activation on indium surfaces, *Nat. Commun.*, 2019, **10**, 892.

56 Y. Zhang, L. Gao, E. J. M. Hensen and J. P. Hofmann, Evaluating the Stability of Co_2P Electrocatalysts in the Hydrogen Evolution Reaction for Both Acidic and Alkaline Electrolytes, *ACS Energy Lett.*, 2018, **3**, 1360–1365.

57 W. Yuan, S. Wang, Y. Ma, Y. Qiu, Y. An and L. Cheng, Interfacial Engineering of Cobalt Nitrides and Mesoporous Nitrogen-Doped Carbon: Toward Efficient Overall Water-Splitting Activity with Enhanced Charge-Transfer Efficiency, *ACS Energy Lett.*, 2020, **5**, 692–700.

58 Y. Ma, Y. An, Z. Xu, L. Cheng and W. Yuan, Activating lattice oxygen of two-dimensional $M_nX_{n-1}O_2$ MXenes via zero-dimensional graphene quantum dots for water oxidation, *Sci. China Mater.*, 2022, **65**, 3053–3061.

This journal is © the Partner Organisations 2023

Inorg. Chem. Front., 2023, **10**, 158–167 | **167**